Hurricane Wind Speed Measurements in Rainy Conditions Using the Airborne Hurricane Imaging Radiometer (HIRAD)

Ruba A. Amarin, *Member, IEEE*, W. Linwood Jones, *Life Fellow, IEEE*, Salem Fawwaz El-Nimri, *Member, IEEE*, James W. Johnson, *Senior Member, IEEE*, Christopher S. Ruf, *Fellow, IEEE*, Timothy L. Miller, and Eric Uhlhorn

***Abstract*—This paper describes a realistic computer simulation of airborne hurricane surveillance using the recently developed microwave remote sensor, the hurricane imaging radiometer (HIRAD). An end-to-end simulation is described of HIRAD wind speed and rain rate measurements during two hurricanes while flying on a high-altitude aircraft. This simulation addresses the particular challenge which is accurate hurricane wind speed measurements in the presence of intense rain rates. The objective of this research is to develop baseline retrieval algorithms and provide a wind speed measurement accuracy assessment for future hurricane flights including the NASA GRIP hurricane field program that was conducted in summer of 2010. Examples of retrieved hurricane wind speed and rain rate images are presented, and comparisons of the retrieved parameters with two different numerical hurricane models data are made. Special emphasis is provided on the wind speed measurement error, and statistical results are presented over a broad range of wind and rain conditions over the full measurement swath (earth incidence angle).**

***Index Terms*—Hurricane imaging, hurricane imaging radiometer (HIRAD), hurricanes wind speed retrievals, synthetic aperture radiometry.**

I. Introduction

AIRBORNE hurricane surveillance, conducted by the National Oceanic and Atmospheric Administration (NOAA) and the U.S. Air Force Reserve 53rd Weather Reconnaissance Squadron, is crucial to hurricane warnings issued by the National Hurricane Center. Flying specially equipped "Hurricane Hunter" aircraft, critical measurements are made of the hurricane eye location, the central pressure, and the maximum sustained (1-min average) surface wind speed. Of these, the surface wind speed is of greatest importance because this is the determining factor in the Saffir–Simpson hurricane scale commonly known as the hurricane category.

For the past two decades, the airborne Stepped Frequency Microwave Radiometer (SFMR) has provided real-time measurements of surface wind speed and rain rates in hurricanes [1]. These measurements are crucial because SFMR is the only remote sensor that is capable of providing continuous measurements of surface wind speeds up to and including Category-5 hurricane conditions. However, there is one disadvantage of SFMR, which is the very narrow measurement swath directly beneath the aircraft.

This paper describes a new sensor technology known as the Hurricane Imaging Radiometer (HIRAD), which has the potential to be the next generation replacement for the SFMR. HIRAD will improve airborne surveillance by imaging surface wind speed and rain rate over a wide swath, which is approximately equal to three times the aircraft altitude. Unlike SFMR's narrow swath, the HIRAD uses synthetic aperture thinned array radiometry technology to create a 1-D microwave imager that synthesizes horizontally polarized brightness temperature, Tb, images cross-track and provides real-aperture imaging along-track [2]. The key to HIRAD's improved performance is its ability to operate as a Fourier synthesis imager at four discrete frequencies (4, 5, 6, and 6.6 GHz) that cover approximately the same C-band octave as the SFMR.

The HIRAD aircraft instrument has been developed over the past 4 years under a NASA Marshall Space Flight Center led collaboration with NOAA's, Atlantic Oceanographic and Meteorological Laboratory, Hurricane Research Division, the Central Florida Remote Sensing Laboratory (CFRSL) at the University of Central Florida and the Space Physics Research Laboratory of the University of Michigan. Fig. 1 shows the HIRAD flight array antenna and flight instrument on the NASA WB-57 pallet that was flown in hurricanes during the summer of 2010.

This paper deals with the evaluation of the HIRAD ability to remotely sense wind speed (primary objective) and rain rate (secondary objective) in hurricanes. Through the use of realistic simulations of hurricane surveillance flights over ocean, we are able to assess the wind speed measurement performance of a conceptual pushbroom wide-band radiometer system that has

Manuscript received July 2, 2010; revised November 17, 2010 and February 14, 2011; accepted May 29, 2011. Date of publication September 15, 2011; date of current version December 23, 2011. This work was supported by the HIRAD Project of the NASA Marshall Space Flight Center under a contract with the Von Braun Center for Science and Innovation.

R. A. Amarin, W. L. Jones, S. F. El-Nimri, and J. W. Johnson are with the University of Central Florida, Orlando, FL 32816 USA (e-mail: ramarin@mail.ucf.edu; ljones@ucf.edu; selnimri@knights.ucf.edu; jwjohnson.8443@gmail.com).

C. S. Ruf is with the University of Michigan, Ann Arbor, MI 48109 USA (e-mail: cruf@umich.edu).

T. L. Miller is with the NASA, Marshall Space Flight Center, Huntsville, AL 35805 USA (e-mail: tim.miller@nasa.gov).

E. Uhlhorn is with the NOAA/AOML/Hurricane Research Division, Miami, FL 33149 USA (e-mail: eric.uhlhorn@noaa.gov).

Color versions of one or more of the figures in this paper are available online at http://ieeexplore.ieee.org.

Digital Object Identifier 10.1109/TGRS.2011.2161637

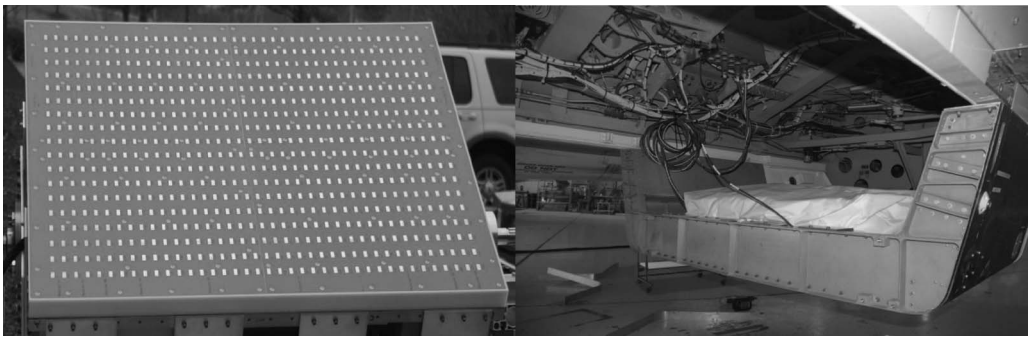

Fig. 1. HIRAD flight array antenna (left panel) and flight instrument integrated on the NASA WB-57 pallet.

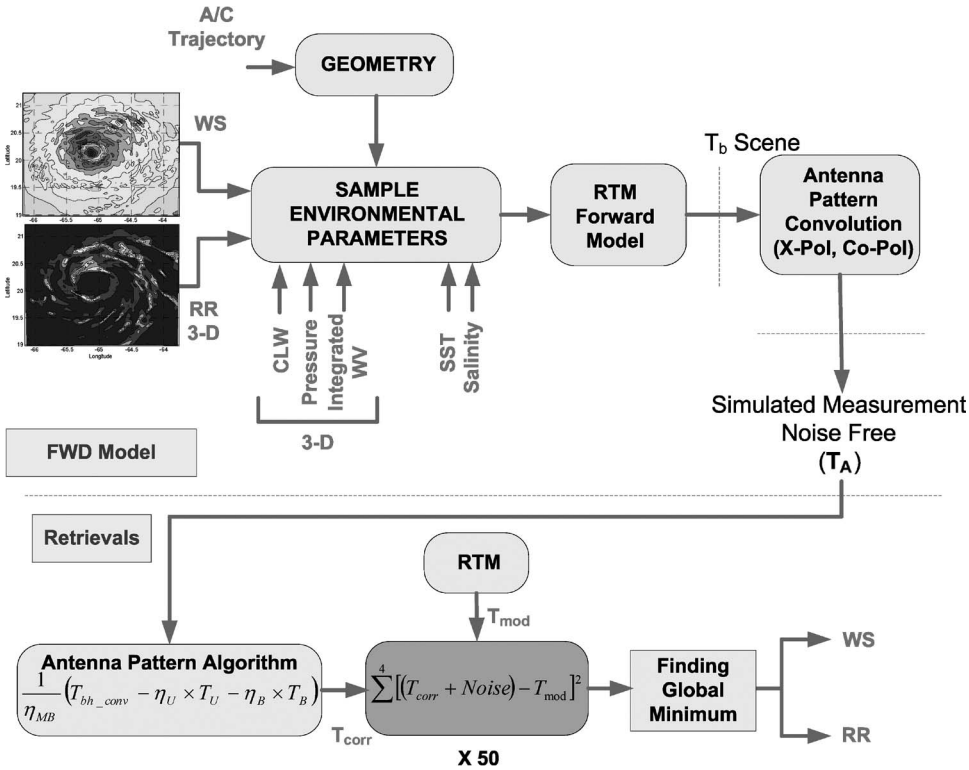

Fig. 2. HIRAD end-to-end simulation.

strong similarities with HIRAD. The goal of this research is to use this simulation to characterize the HIRAD hurricane surface wind speed measurement accuracy as a function of wind speed, rain rate, and cross-swath location earth incidence angle (EIA). We use proven methods of microwave radiometer measurement modeling in a Monte Carlo simulation to predict wind speed retrieval errors parametrically with realistic instrument errors, and the results of the simulation are directly applicable to the estimation of HIRAD performance.

II. Approach

A HIRAD end-to-end computer simulation, shown in Fig. 2, has been developed for hurricane wind speed measurement performance evaluation. The simulation begins with geometry calculations where the cross-track locations of the antenna beam lines-of-sight are calculated as the aircraft, operating at 20 km altitude, transects the storm in radial cuts through the eye. To provide a realistic set of 3-D environmental parameters,

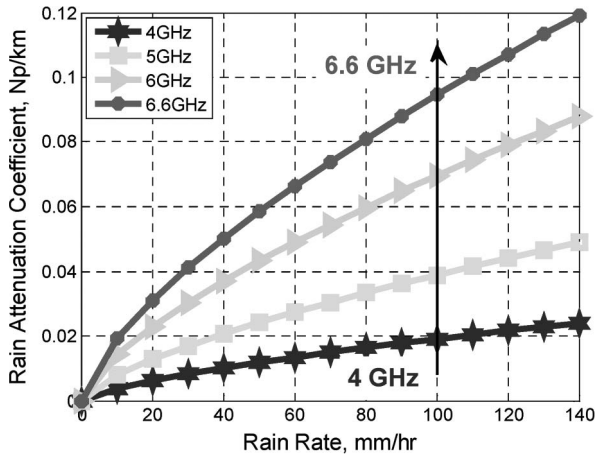

Fig. 3. Rain absorption coefficients for HIRAD frequencies.

several numerical hurricane models are run, from which simulated HIRAD Tb's are derived using a forward radiative transfer model (RTM). This RTM includes the SFMR rain absorption

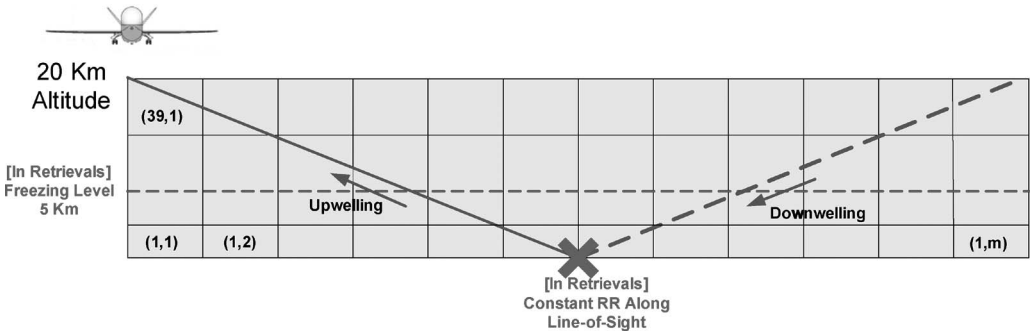

Fig. 4. Geometry for the atmospheric path integration used in the forward RTM and the retrieval algorithm simulation.

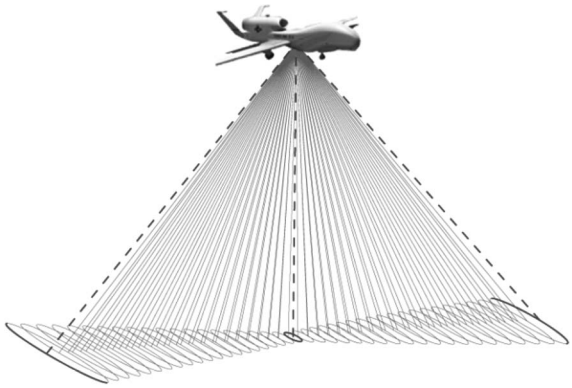

Fig. 5. Equivalent real-aperture pushbroom radiometer system with 41 beams cross-track.

model for the hurricane environment, and an ocean surface emissivity model developed particularly for high wind speeds and HIRAD high incidence angle measurements [3]. The antenna temperature is then computed by convolving the scene brightness temperature, over a spherical surface surrounding the antenna, with the antenna gain pattern. Finally, these simulated antenna temperature measurements, with expected errors, are used in a geophysical retrieval algorithm with realistic sources of random errors that are expected in aircraft observations. Here, the retrievals are performed, using a Monte Carlo simulation, to infer hurricane ocean surface wind speed and rain rate.

Afterwards, the retrieved results and nature runs are compared and statistically analyzed to determine differences (errors), which are characterized as a function of the mean nature run wind speed and rain rate and as a function of cross-track location (incidence angle).

III. Hurricane Forward Radiative Transfer Model Simulation

This section addresses the forward RTM model that was developed for this study along with a description of the simulated real-aperture pushbroom radiometer equivalent of HIRAD and the derivation of the convolved brightness temperature.

A. Forward Radiative Transfer Model

As part of the HIRAD development, the CFRSL RTM was modified for hurricane environment. The selected approach was to use the SFMR rain absorption algorithm and to use the improved microwave radiometric ocean surface emissivity model that was specifically developed for HIRAD [3]. This C-band ocean surface emissivity model extends current model capabilities to hurricane force wind speeds over a wide range of incidence angles. It was primarily developed using C-band brightness temperature observations during hurricanes, which were obtained using the airborne SFMR measurements at nadir and off-nadir (collected during aircraft banks).

The CFRSL ocean surface emissivity model adopted a physical-based model formulation with empirical coefficients that divided the total emissivity into two parts, foam and foam-free rough ocean, as shown in

$$\varepsilon_{ocean} = FF \times \varepsilon_{foam} + (1 - FF)\varepsilon_{rough} \tag{1}$$

where ε_{ocean} represents the total ocean emissivity, ε_{foam} is the foam emissivity (depends on wind speed, EIA, and frequency), FF is the foam fraction (% area covered by foam—depends on wind speed only), and ε_{rough} is the rough ocean emissivity, which depends on both the polarized smooth surface Fresnel power reflection coefficients and the degree of surface roughness as given by

$$\varepsilon_{rough} = \varepsilon_{smooth} + \Delta\varepsilon_{excess} \tag{2}$$

where ε_{smooth} is the specular emission given by (3) using the air-to-ocean Fresnel power reflection coefficient (Γ), and $\Delta\varepsilon_{excess}$ is the excess emissivity, which depends on the wind speed, SST, frequency, polarization, and incidence angle

$$\varepsilon = 1 - \Gamma. \tag{3}$$

The CFRSL RTM described by Hong [4] is used to compute the absorption coefficients for water vapor, cloud liquid water, and oxygen. For the HIRAD frequencies, both the water vapor and cloud liquid absorption in hurricanes are significant, but oxygen and ice absorption is negligible. Further, rain is the dominant atmospheric absorber, but fortunately, at HIRAD's long operating wavelengths, scattering is not significant even for high rain rates. Therefore, this RTM is modified to include the absorption/emission effects of rain, which are derived from the work of Jorgensen and Willis [5] and Olsen *et al.* [6] according to (4).

$$k_R = gf^{3.2}\boldsymbol{R}^b \tag{4}$$

where k_R is the rain absorption coefficient in Np/km, $g = 9.4 \times 10^{-6}$ Np/km, f is the radiometer frequency in GHz, R

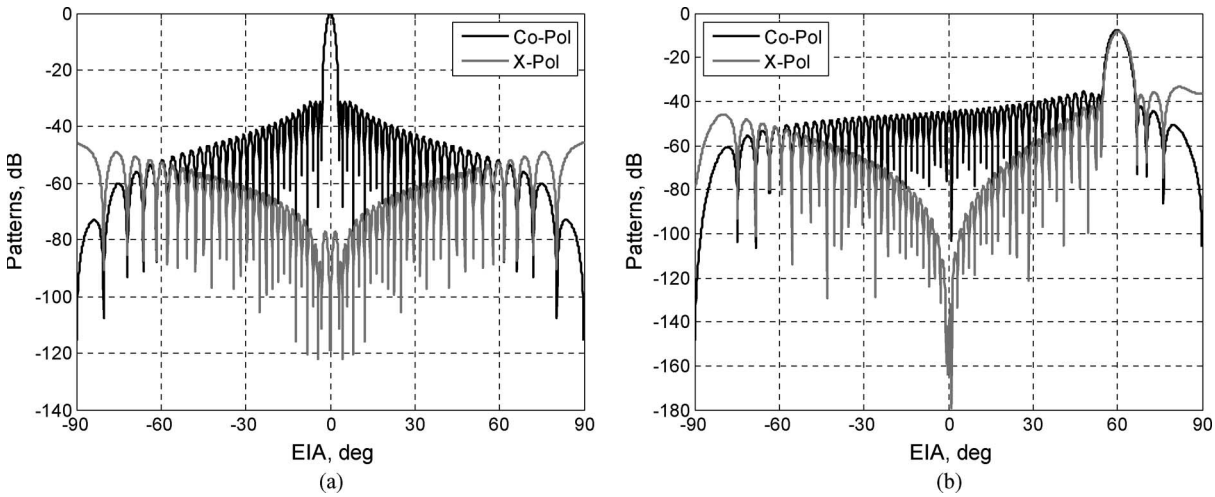

Fig. 6. Co-Pol and X-Pol patterns at 6.6 GHz frequency for (a) 0 deg and (b) 60 deg scan beams.

is the rain rate in mm/h, and the exponent "b" $= 0.69$. Fig. 3, is a plot of the rain rate absorption coefficient for the HIRAD frequencies according to (4).

These SFMR rain coefficients were derived by Swift *et al.* [7] and are currently used by the operational SFMR retrieval algorithm. Unfortunately, the lack of rain rate surface truth measurements in hurricanes has prevented validation of the SFMR rain retrievals. Nevertheless, for HIRAD, we have higher confidence in the frequency dependence of rain absorption than we do in its absolute value of emission. Because of our multifrequency retrieval algorithm, we can estimate the optical depth and emission due to rain, and hence properly correct for this in our wind speed retrievals. What we cannot do well is estimate the actual rain rate that corresponds to that emission and attenuation.

For the hurricane environmental parameters required by the forward RTM, two hurricane numerical model "nature run" simulations were used in this paper. First was the Penn State-NCAR fifth-generation Mesoscale Model (MM5) described by Chen *et al.* (2007) [8], and the second was the Weather Research and Forecasting (WRF) model used by NOAA, HRD [9]. These two model runs for Hurricane Frances (MM5, 2004) and Hurricane Bill (WRF, 2009) provided realistic 3-D environmental parameters (rain, water vapor, clouds, and surface winds) from which simulated HIRAD Tb's are derived for typical aircraft flight patterns. Further, the simulation included a high-resolution SST field that was provided by the National Space Science and Technology Center (NSSTC) [10].

The 3-D structure of the hurricane numerical model was mapped into 39 atmospheric layers in the vertical and into a 2-D ocean surface (1.67 km pixels corresponding to the nature run resolution). The simulated HIRAD Tb's were calculated along the slant path as shown in Fig. 4, whereby the upwelling and downwelling emission components were calculated along separate specular reflection slant paths.

B. HIRAD Equivalent Pushbroom Radiometer

In this paper, results are presented for a simulated real-aperture pushbroom radiometer equivalent of HIRAD, which is shown in Fig. 5. In the simplest terms, the equivalent system replaces the HIRAD Synthetic Thinned Array Radiometry (STAR) [11] imaging with 41 individual antenna beams. These beams are equivalent in terms of the C-band operating frequencies, approximate antenna pattern spatial resolutions, cross-track boresight pointing angles (with boresights spaced on 3 deg centers ± 60 deg), and horizontal polarization. The approach of using a pushbroom radiometer system to model the HIRAD measurement performance has the advantage of simplicity of the simulation, which employs well-proven microwave radiometry techniques [12].

C. Antenna Brightness Temperature

The pushbroom antenna beams were implemented as four independent antenna designs (one per frequency) that were electronically steerable phased arrays that produced similar patterns to the synthesized beams for HIRAD. Both the H-Pol and V-Pol apparent Tb scenes were convolved with the copolarized (Co-Pol) and cross-polarized (X-Pol) antenna patterns, respectively, and the convolved H-Pol and V-Pol Tb's are:

$$T_{bH_{conv}} = \frac{\int_0^{2\pi}\int_{-\theta_1}^{\theta_1} T_{aph}(\theta,\phi)\times F_{Co-Pol}(\theta,\phi)\times sin\theta d\theta d\phi}{\int_0^{2\pi}\int_{-\theta}^{\theta} F_{Co-Pol}(\theta,\phi)\times sin\theta d\theta d\phi} \quad (5)$$

$$T_{bV_{conv}} = \frac{\int_0^{2\pi}\int_{-\theta}^{\theta} T_{apv}(\theta,\phi)\times F_{X-Pol}(\theta,\phi)\times sin\theta d\theta d\phi}{\int_0^{2\pi}\int_{-\theta}^{\theta} F_{X-Pol}(\theta,\phi)\times sin\theta d\theta d\phi}. \quad (6)$$

In (5), the horizontally convolved Tb is integrated over $\pm\theta_1 = \pm 30$ deg that results in $\sim$100% beam efficiency for the Co-Pol antenna pattern, but for the X-Pol pattern, the θ limits in the vertically convolved Tb given by (6), change by beam position to insure $> 90\%$ beam efficiency.

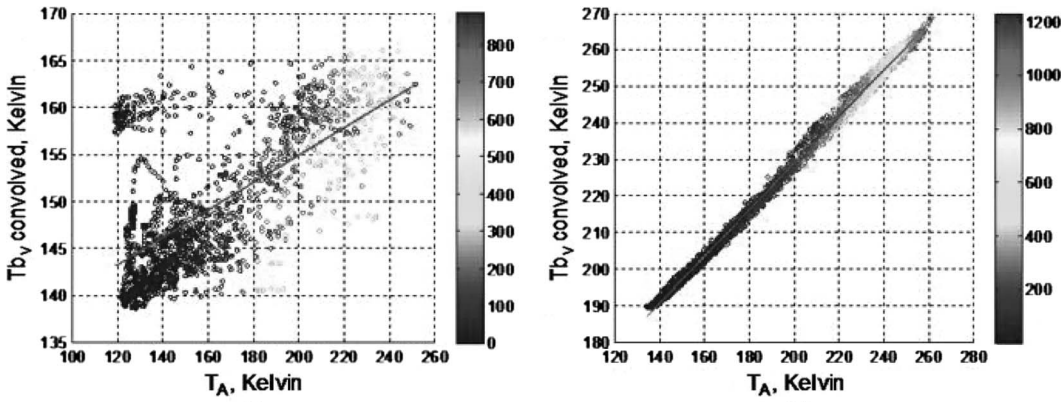

Fig. 7. Correlation of T_A and T_{bVconv} brightness temperatures for 6.6 GHz for (a) nadir and (b) ± 60 deg (left and right sides of HIRAD swath combined). The color-bar refers to the integrated RR values in km-mm/h.

The final convolved brightness temperature T_A is a superposition of T_{bHconv} and T_{bVconv} according to,

$$T_A = (1-\gamma)T_{bH_{conv}} + \gamma T_{bV_{conv}} \tag{7}$$

where γ is the ratio of the X-Pol brightness temperature to the total and is approximated by [see Eq. (8), shown at the bottom of the page].

γ increases with incidence angle (beam position) for each frequency. For example, at nadir [Fig. 6(a)], γ is approximately zero, but at 60 deg [Fig. 6(b)], Co-Pol and X-Pol patterns have the same power gain, making $\gamma \sim 0.5$.

IV. Geophysical Retrieval Algorithm

The HIRAD geophysical retrieval algorithm is used to estimate hurricane ocean surface wind speed and rain rate using the statistical least-squares difference method. In this procedure, the retrieved wind speed and rain rate at a surface pixel are those values that minimize the difference between the HIRAD Tb measurements and modeled apparent brightness temperatures for the four HIRAD frequencies.

A. Retrieval RTM

The HIRAD geophysical retrieval algorithm uses a RTM that is different than the "forward RTM" used in the simulation of HIRAD antenna temperatures. The differences are primarily associated with the input environmental parameters used. For the ocean SST, the retrieval assumes a constant SST (28 °C), whereas the forward model uses an actual high resolution SST field. The surface wind speed is the retrieved parameter at a cross-track pixel, whereas it is known from the nature run for the forward model.

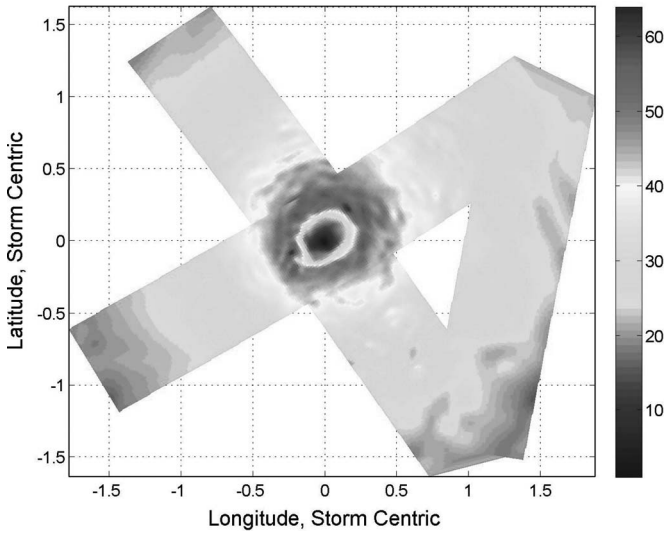

Fig. 8. Example of a simulated HIRAD wind speed image for a typical aircraft flight track from an altitude of 20 km. The wind field is from Hurricane Frances with color bar in m/s.

For the atmosphere, the retrieval assumes a 2-D hurricane climatological model (vertical profiles that vary with radial distance from the hurricane center). The surface rain rate is a retrieved parameter at each cross-track pixel, but the retrieval model assumes that the rain is uniformly distributed from the freezing level (5 km altitude) to the surface. Further, the retrieval RTM calculates the upwelling and downwelling Tb based upon the surface rain rate. Since both the surface wind speed and rain rate are retrieved parameters, the T_{mod} is calculated parametrically with rain rate (0–100 mm/h) and wind speed (0–80 m/s) and stored in a matrix for each frequency and incidence angle.

$$\gamma = \frac{\int\limits_{\text{First Nulls}} F_{X-Pol}(\theta,\phi) \times \sin\theta d\theta}{\int\limits_{\text{First Nulls}} F_{X-Pol}(\theta,\phi) \times \sin\theta d\theta + \int\limits_{\text{First Nulls}} F_{Co-Pol}(\theta,\phi) \times \sin\theta d\theta} \tag{8}$$

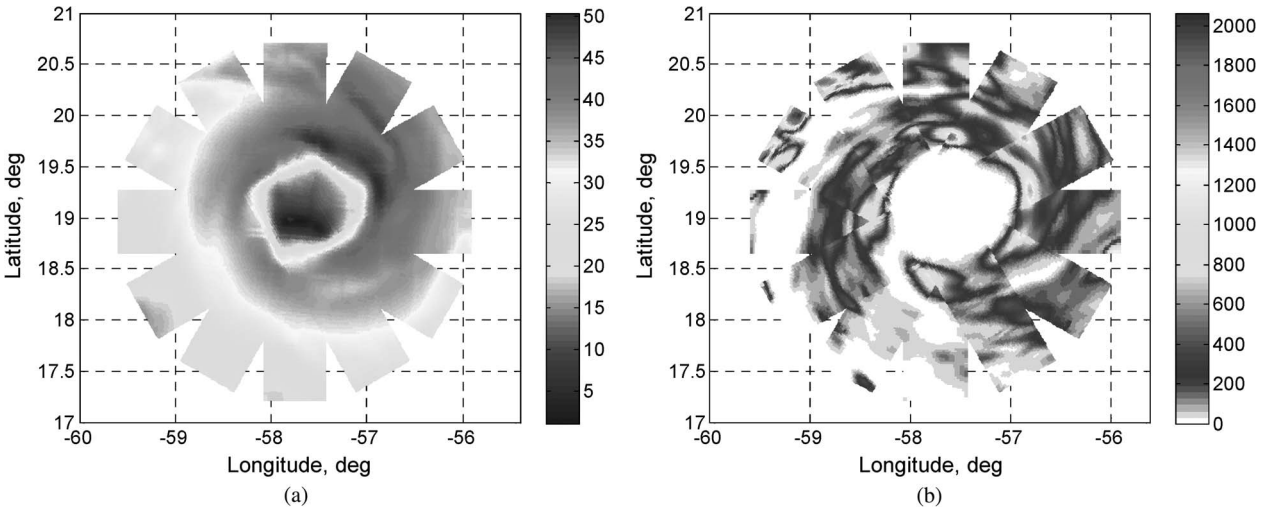

Fig. 9. Hurricane Bill nature run (a) wind speed (m/s) and (b) integrated rain rate (km-mm/h) for six flight legs.

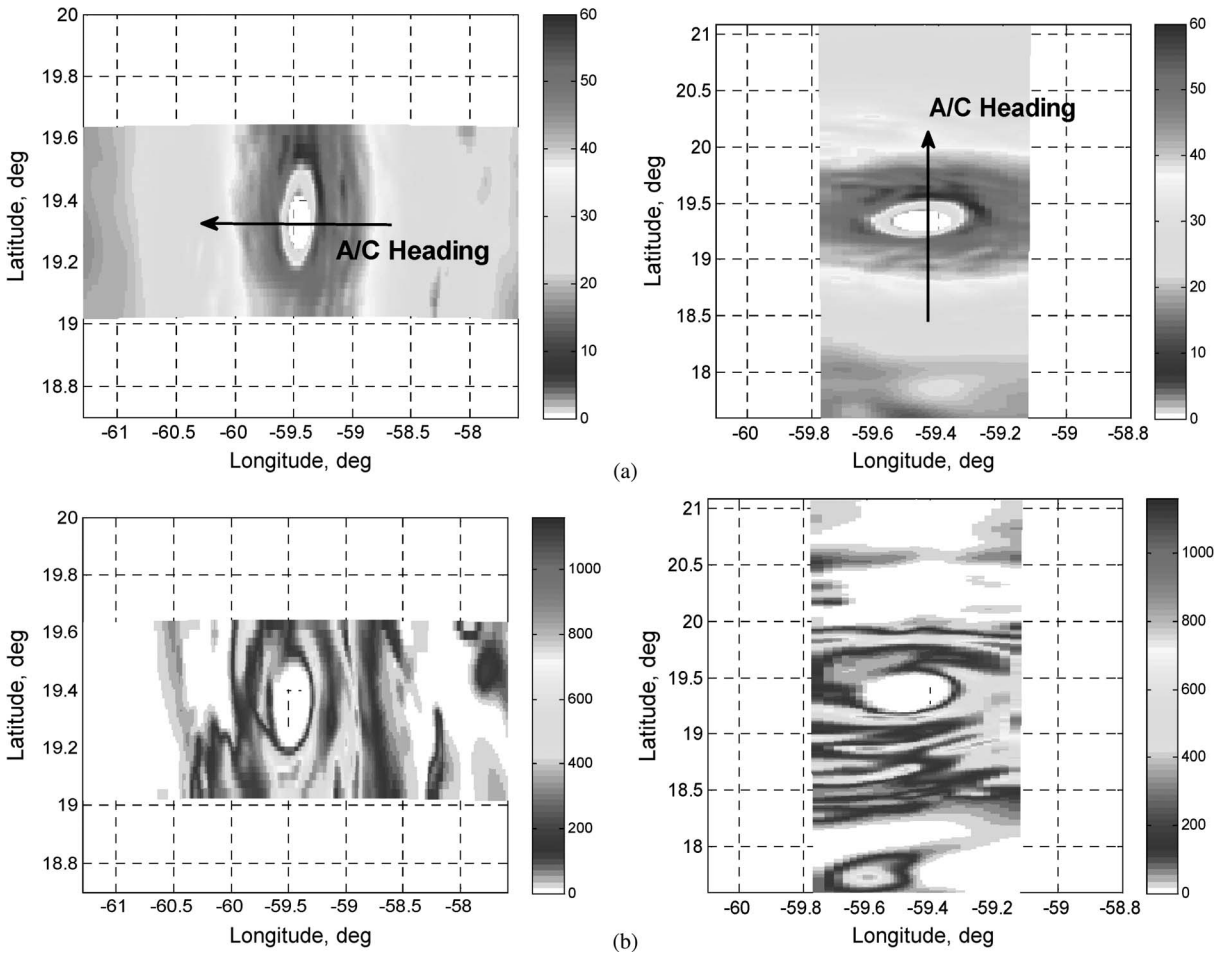

Fig. 10. Hurricane Frances nature run (a) wind speed (m/s) and (b) integrated rain rate (km-mm/h) for Leg 1 (left panel) and Leg 2 (right panel).

B. Antenna Pattern Correction

The HIRAD measures the antenna temperature, but the retrieval algorithm requires the "true" brightness temperature at the antenna boresight; therefore, the antenna pattern correction algorithm is used to correct for the effects of the antenna cross polarization coupling and the antenna pattern (sidelobes) convolution with the scene Tb.

First, the cross polarization leakage ($T_{bV_{conv}}$) was removed from the total antenna brightness temperature (T_A) computation according to

$$T_{bH_{conv}} = \frac{T_A - \gamma \times T_{bV_{conv}}}{(1-\gamma)}. \tag{9}$$

Unfortunately, in an actual HIRAD measurement, the hurricane Tb scene is unknown; so this algorithm must use

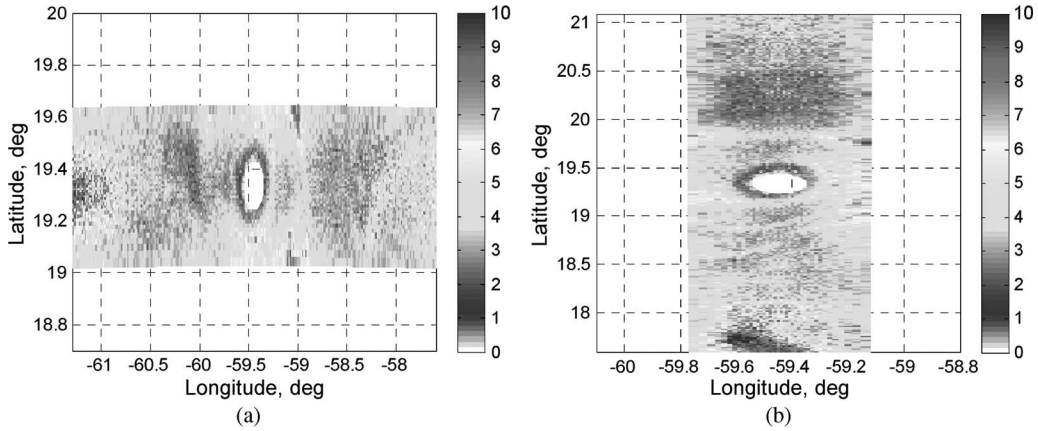

Fig. 11. Hurricane Frances RMS retrieved wind speed errors (m/s) for (a) Leg 1 and (b) Leg 2.

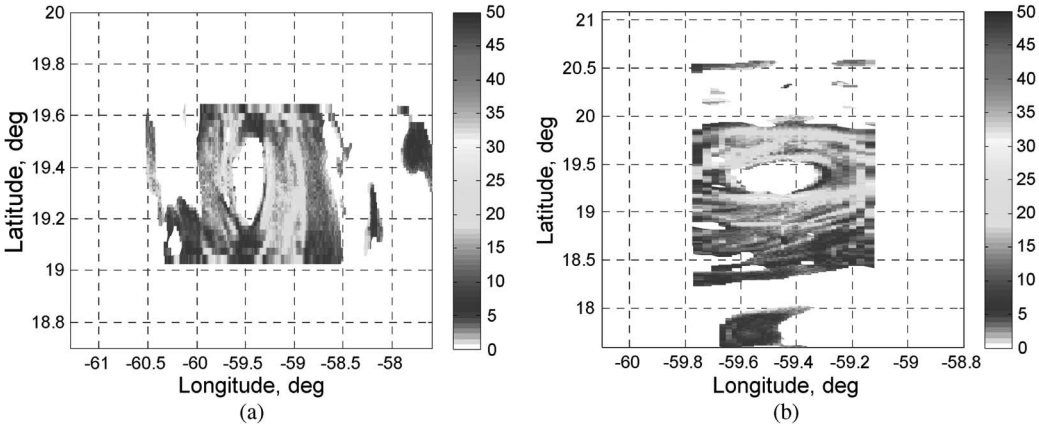

Fig. 12. RMS retrieved integrated rain rate errors (%) for (a) Leg 1 and (b) Leg 2.

estimates for the T_{bVconv}. To generate these values, a hurricane simulation was performed to determine the correlation between the measured antenna temperature (T_A) and the corresponding convolved V-Pol brightness temperature (T_{bVconv}). Using the forward RTM, simulated HIRAD Co-Pol and X-Pol convolved Tb's were obtained over the entire hurricane. Next, the T_{bVconv} values were cross-correlated with the corresponding HIRAD T_A's. Separate regression analyses were performed for each beam position, and the results indicated that a robust linear relationship existed between T_A and T_{bVconv} (see typical results shown in Fig. 7 for nadir and 60 deg for 6.6 GHz). A weaker correlation exists at near nadir angles (panel-a) as seen by the increased variance about the linear-fit, but this does not significantly affect the Tb correction since the cross-polarized coupling γ is small ($\sim$ zero) near these angles. Hence, these linear relationships were used to estimate the T_{bVconv} at each beam position.

After removing the X-Pol leakage, the following antenna pattern correction was applied:

$$T_{Corr} = \frac{1}{\eta_{ML}} \left[T_{bH_{conv}} - \eta_U \times T_U - \eta_B \times T_B \right] \qquad (10)$$

where T_U and T_B are the brightness temperature contributions that correspond to the "up—above the boresight" and "below the boresight" portions of the pattern, respectively. In a similar manner as the X-Pol leakage, these sidelobe brightness contributions were estimated by cross-correlation with the simulated measured H-Pol antenna temperature. The antenna beam efficiencies of the main lobe (η_{ML}), above the boresight (η_U), and below the boresight (η_B) are derived from the HIRAD antenna patterns.

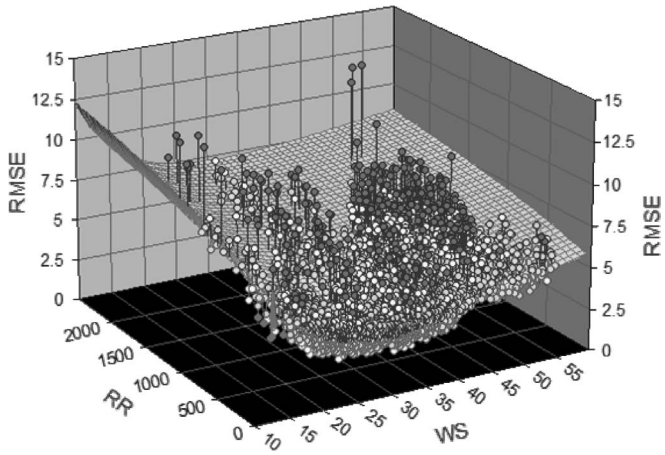

Fig. 13. RMS retrieved wind speed error surfaces (m/s) for 60 deg (left and right sides of HIRAD swath combined).

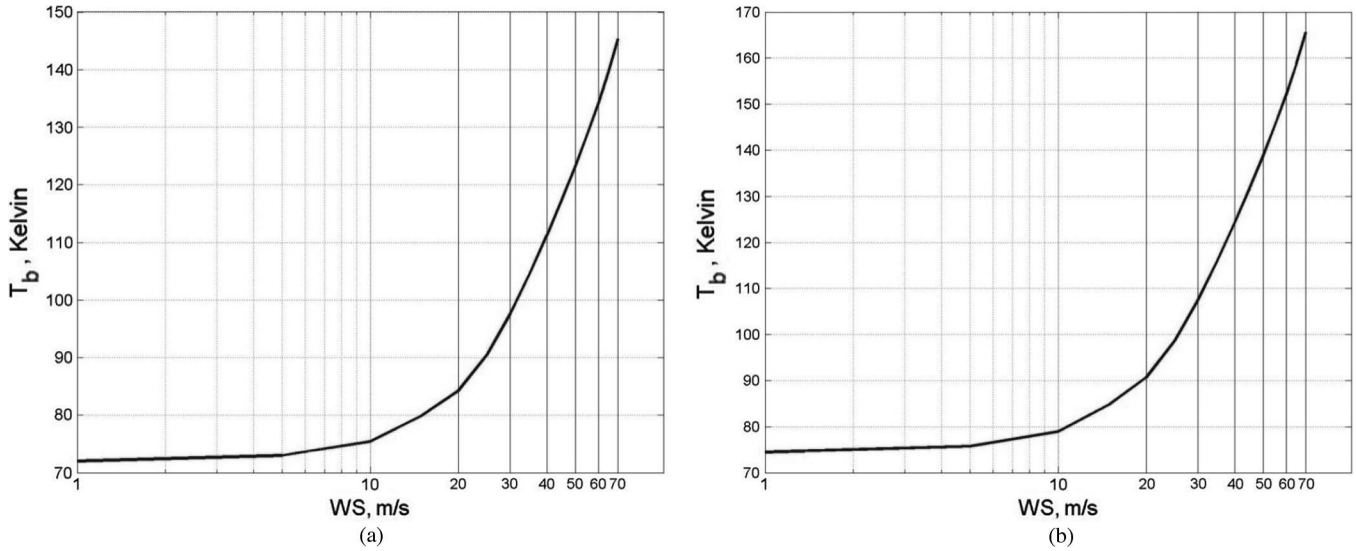

Fig. 14. Ocean brightness temperature sensitivity to wind speed at an EIA of 53 deg. (a) 4 GHz. (b) 6.6 GHz.

C. Retrieval Algorithm

Referring to Fig. 2, after correcting for antenna pattern effects, a Monte Carlo retrieval simulation was run, and the RMS retrieval error was calculated (compared to the nature run). Three main sources of errors are modeled in the retrieval module, namely: the instrument Tb errors (noise equivalent delta-T (NEDT) and the receiver gain fluctuations (ΔG/G)), the errors associated with aircraft attitude variations, and the geophysical model function (emissivity model) errors. In the simplest terms, these Tb errors are modeled as additive zero-mean Gaussian random distributions with standard deviations that we vary parametrically from 1 to 8 Kelvin. We use this large range of RMS random errors to assess the sensitivity of the retrieval to random error, but for HIRAD, the expected total random error is estimated to be 2–4 Kelvin.

In the retrieval module, the modeled brightness temperature matrix T_{mod} is compared to the corrected brightness temperature with random errors added $(T_{corr} + Noise)$ at each of the four frequencies. Each element in the difference matrices is squared, and the algorithm searches for the local minimum of the summed squared difference surface, over all frequencies using the statistical least-square difference method according to (11) to retrieve ocean surface wind speed and rain rate. This process is repeated 50 times in a Monte Carlo simulation for each beam position in all HIRAD cross-track scans to collect root mean square error (RMSE) statistics

$$\sum_{i=1}^{4} \left[(T_{\rm corr} + Noise)_i - (\hat{T}_{\rm model})_i \right]^2. \qquad (11)$$

V. Results

A. Retrieved Wind Speed and Rain Rate Error Statistics

Comprehensive simulations for assessing HIRAD performance were conducted using wind and rain fields from numerical model "nature runs" for hurricanes Frances and Bill. The objective of this analysis was to provide realistic imaging simulations, compile a relatively large data set of measurements, with errors, and demonstrate potential HIRAD performance over the full swath by mapping brightness temperature errors to estimate wind speed and rain rate. The most common flight pattern used is the "Fig-4" where the aircraft flies two passes, normal to each other, through the center of the eye as presented in Fig. 8.

A single Fig-4 flight pattern, with two perpendicular flight legs through the eye of a hurricane 90 deg apart would adequately cover the inner portion of the hurricane and measure the maximum winds. However, to build a larger data set for this error analysis, three Fig-4 patterns were simulated, with six flight legs 30 deg apart, as in Fig. 9 per hurricane, and two legs outside the eye to capture high rain bands at relatively low wind speed values were added. Each flight leg is made up of 240 individual HIRAD scans, resulting in a total of 3840 scans over the HIRAD swath for the 16 legs. The simulated HIRAD swath consists of 41 individual measurements of Tb, and the Monte Carlo simulation adds zero-mean Gaussian random errors, with a STD varied parametrically for 1, 2, 4, and 8 Kelvin cases, to these measurements. Fifty trials for each case and 3840 scans comprise the whole data set for the error analysis. The nature run from the numerical hurricane model serves as surface truth, which is compared to the retrieved wind speed and rain rate values, and RMS errors are computed from the differences.

Hurricane Frances wind (m/s) and the integrated rain (km-mm/h) fields for two legs in a Fig-4 are illustrated in Fig. 10, where the left panel represents Leg 1 (aircraft flying west along a constant latitude) and the right panel represents Leg 2 (aircraft flying north along a constant longitude). Note that both legs are plotted on different latitude and longitude scales. The maximum wind speed is $\sim$60 m/s in the eye wall region of the hurricane, and the maximum integrated rain rate is $\sim$1100 km-mm/h at the edges of the swath, which translates to $\sim$110 mm/h assuming a slant rain path of 10 km.

Corresponding wind speed and integrated rain rate error images are plotted for the orthogonal legs in Figs. 11 and 12, respectively for the 4 Kelvin random error case. The color-bar

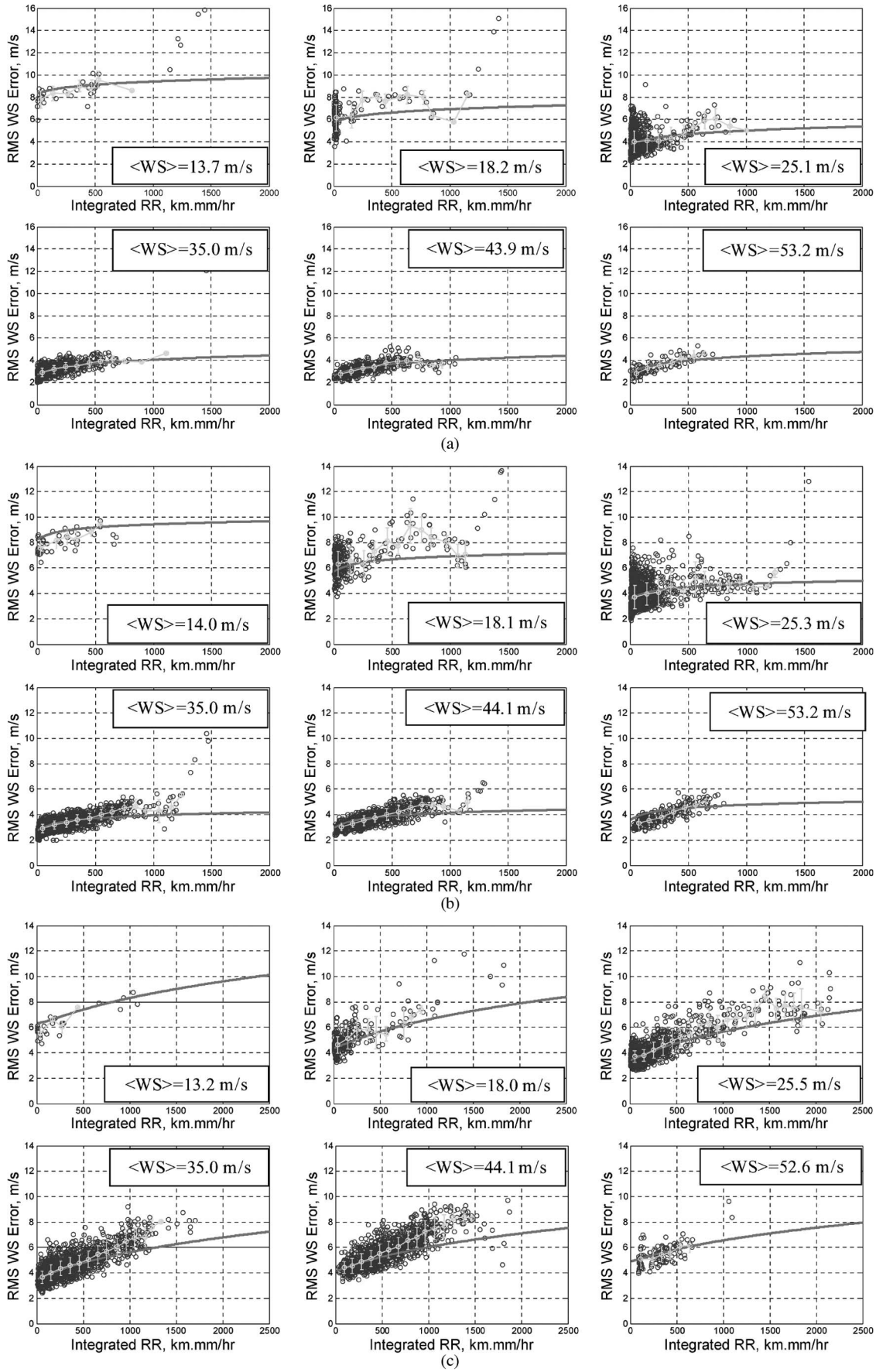

Fig. 15. RMS wind speed errors (m/s) at EIAs: (a) nadir, (b) 30 deg, and (c) 60 deg for six wind speed bins ±5 m/s. (a) nadir. (b) 30 deg (left and right sides of HIRAD swath combined). (c) 60 deg (left and right sides of HIRAD swath combined).

represents the RMS retrieved error in m/s, and note that in Fig. 11, the highest wind speed errors are primary associated with rain bands, particularly in the eye wall region where the rain is the most intense and at the edges of the swath where slant path lengths are greatest. Further, heavy rain, even near nadir, can cause significant wind speed errors as seen in Fig. 11(a) at 59.5 deg longitude and in (b) at 17.5 deg latitude (bottom of image).

Results presented in Fig. 12 indicate that the retrieved integrated rain rates agree well over most of the image and that the highest errors (50%) occur at the swath edge and more typically the errors are between 10% and 30%. However, the reader is cautioned that these results may be optimistic, given the lack of validation for the SFMR rain absorption coefficients upon which these simulations are based.

To characterize the wind speed retrieval error as a function of wind speed, rain rate, and cross-track beam position (EIA), a 2-D regression analysis was performed for fixed incidence angles. Results presented in Fig. 13 show the best-fit wind speed RMSE surface (based on maximizing "coefficient of determination") for the 60 deg beam position and 4 K random error. Each symbol represents an individual pixel estimate of the RMS wind speed error, and these are color coded with blue bordered circles indicating points above the surface, red bordered circles indicating points below the surface and filled circle colors indicating the relative distance of these points from the surface.

The shape of the wind speed RMSE surface is similar at all EIAs, which indicates a similar error dependence on wind speed and rain rate. At low wind speeds (< 15 m/s), the error is a maximum because of the nature of the geophysical model function, where the Tb sensitivity to wind speed is weakest as illustrated in Fig. 14. For higher wind speeds the RMSE decreases until $\sim$25 m/s after which the error is approximately constant [13]. With respect to rain rate, the lowest RMSE is rain-free, and the error monotonically increases thereafter. At higher incidence angles, the RMSE monotonically increases due to higher rain attenuation coming from longer slant path lengths.

An alternate way to examine the error characteristics is presented in Fig. 15 by binning the HIRAD measurement pixels by surface truth wind speed bins and plotting the corresponding RMSE pixels against the corresponding surface truth integrated rain rate. These comparisons are presented in separate panels for EIAs of 0, 30, and 60 deg, where the solid curve corresponds to the best-fit RMSE surface. Also, shown in Fig. 15 are the binned average and STD of RMSE calculated in integrated rain rate bins.

Finally, we compare the wind speed error statistics of HIRAD to those of SFMR in Fig. 16. We believe that this result supports the fidelity of our simulations (at least for the near nadir EIAs). The basis of this comparison comes from Uhlhorn and Black [14], which evaluated SFRM wind speeds against independent surface-adjusted GPS dropsonde winds that were acquired in 2 years of flight experiments by the NOAA Hurricane Research Division. Basically, Fig. 16 is from the Uhlhorn and Black paper with the HIRAD near nadir wind speed RMSE error surface (compared to the nature run surface truth) superimposed for zero rain and 500 km-mm/h integrated rain rate cases. The HIRAD error model produces a very reasonable fit with these independent SFMR wind speed comparisons with dropsondes.

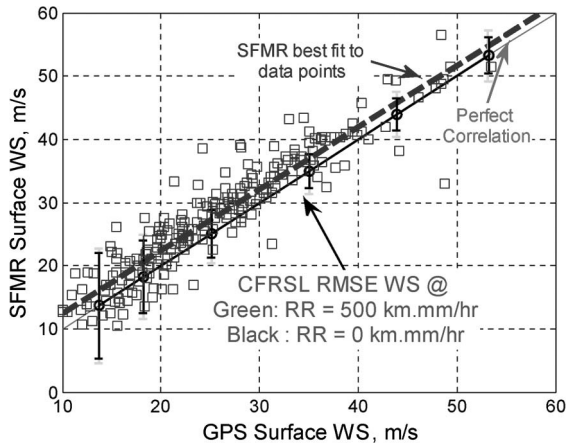

Fig. 16. CFRSL RMS wind speed error comparisons with SFMR at nadir [14].

B. Individual Error Source Assessment

An understanding of each error source and its contribution to the total error in retrieved wind speed is necessary and provides a basis for future improvements to the retrieval algorithm. The error source assessment consisted of evaluating each of the following five error sources individually: sea surface temperature, rain, atmosphere, antenna pattern, and random errors. In each case, we turned on one error source at a time to study its contribution to the RMS wind speed errors. Data from one leg only (constant longitude) in Fig. 10 was used in this analysis.

The purpose of the "Perfect Retrieval" study is to demonstrate that an error-free retrieval will reproduce the surface truth exactly. This was done by considering a zero random error case, including no atmospheric or rain effects, adding no cross-pol or sidelobe contributions, and keeping SST constant. The simulation was run for Hurricane Frances (surface wind only) over the aircraft Leg 1 [Fig. 17(a)]. The magnitude of the wind speed errors does not go beyond 0.05 m/s which represent the quantization errors due to the wind speed step size of 0.1 m/s in the retrieval algorithm as shown in Fig. 17(b).

The "imperfect SST knowledge" study investigated the effect of assuming a constant SST in the retrievals compared to the real SST field used in the FWD model. The magnitude of the error is small, less than 0.5 m/s, and is maximum where there are relatively low wind speeds (less than 20 m/s) and larger SST variation as shown in Fig. 17(c). These errors are included in the statistics presented for the noise-free (zero random error) case.

The "rain errors" study investigated the effect of using a constant rain rate along the antenna line of sight in the retrievals versus the true 3-D variation in rain rate. The maximum errors, of 5 m/s, were in regions of heavy rain and at the edges of the swath, which is expected due to the longest slant path. Errors of 3 m/s were seen in midregions of the swath with heavy rain. Near nadir, RMS wind speed errors are due to the vertical variation in rain rate [Fig. 17(d)]. The spatial distribution of the wind speed errors follows the rain pattern, but it is also

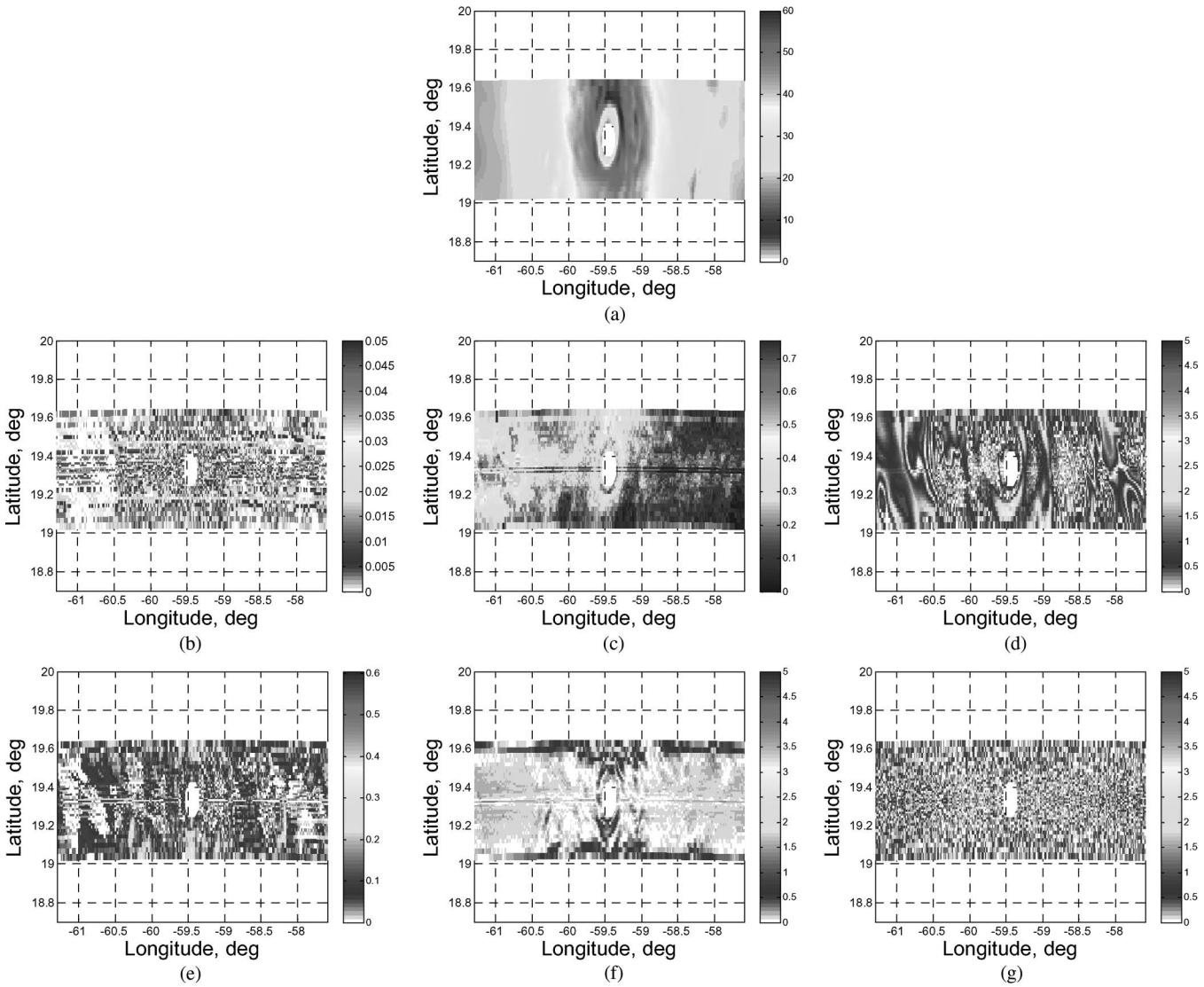

Fig. 17. For Frances Leg 1 (a) surface wind field (m/s) and RMS wind speed errors (m/s) for studying (b) perfect retrieval (c) imperfect SST knowledge (d) rain errors (e) imperfect atmosphere parameter knowledge (f) antenna pattern correction errors and (g) random errors.

modulated by the mean wind speed. For example, these errors are reduced where the GMF has a greater wind speed sensitivity $(\mathrm{dT_b/dWS})$.

The "imperfect atmosphere parameter knowledge" study investigated the effect of using an a priori climatological hurricane model for the atmosphere in the retrievals, rather than the true 3-D atmosphere. As noticed from Fig. 17(e), the magnitude of the error is small, less than 0.5 m/s, and is maximum at the edges of the swath where path lengths are the greatest. Errors of this magnitude are within the statistics presented for the noise-free (zero random error) case.

The "antenna pattern correction errors" study investigated the effect of using the algorithms developed in Section IV, for correcting for the cross-pol contribution and antenna pattern sidelobes, in the retrievals. The error is maximum at the edges of the swath due to the larger X-Pol contribution ($\sim$50%), but for the most part is between $0 \sim 0.25$ m/s where the GMF has a strong slope, $\mathrm{dT_b/dWS}$ as shown in Fig. 17(f).

The purpose of the "random errors" study is to demonstrate the effect of adding random error to the simulation. This was done by adding random errors of 1 Kelvin, including no atmospheric or rain effects, adding no cross-pol or sidelobe contributions, and keeping SST constant. As shown in Fig. 17(g), the error follows a uniform trend across the whole swath. There are no visible patterns other than the hurricane eye. The errors are less than 1 m/s, and there are no edge of swath or path length-dependent features. It is expected that at lower wind speeds ($<$ 20 m/s), the RMS wind speed errors will increase due to the nature of the GMF.

VI. Summary and Conclusion

The HIRAD instrument concept has the potential to dramatically improve the state of the art for airborne hurricane surface wind speed measurements that are currently provided by SFMR. This improved HIRAD capability to provide wide swath measurements of ocean wind speed in the presence of strong rain rates can make very significant positive impact on hurricane forecast by the NOAA National Hurricane Center.

The HIRAD simulation presented in this paper is composed of a forward RTM, to calculate realistic brightness temperature measurements in a 3-D treatment of the atmospheric components and rain, and a statistical least-squares difference inversion algorithm, which was based on the HIRAD geometry and the antenna design. Nature, or surface truth, was represented using the highly realistic MM5 and WRF numerical model runs for wind and rain fields for hurricane Frances, 2004, and hurricane Bill, 2009, respectively.

Monte Carlo error studies were conducted for simulated HIRAD surveillance flights in hurricanes Frances and Bill. Sixteen flight lines were simulated to provide complete images of Frances with assumed random brightness temperature errors of 1, 2, 4, and 8 Kelvin applied. The modeled surface truth and the simulated retrievals were compared and the resulting differences or RMSE for wind speed were computed in the presence of rain. It was observed that the retrieved wind speed compares well to the surface truth over most of the swath; however, the increased slant path near the edges of the swath and antenna pattern effects and limitations to the treatment of rain in the retrieval algorithm did produce increased wind speed errors at swath edges. The wind speed retrieval error was further characterized as a function of wind speed, rain rate, and beam position (EIA), by computing wind speed error surfaces. These relationships showed that the shape of the RMSE surface is similar at all EIAs, but the magnitude of the wind speed error increases slightly with increasing EIA. This effect is probably due to the increased slant path that significantly reduces the atmospheric transmissivity through rain. The RMS wind speed errors are the greatest at lower wind speeds (< 15 m/s), due to the decreased sensitivity of the ocean emissivity GMF with respect to wind speed $(\mathrm{dT_b/dWS})$, and this is true at all beam positions.

ACKNOWLEDGMENT

This work was sponsored under Grants from the Von Braun Center for Science and Innovation, Huntsville, AL.

REFERENCES

[1] E. W. Uhlhorn, P. G. Black, J. L. Franklin, M. Goodberlet, J. Carswell, and A. S. Goldstein, "Hurricane surface wind measurements from an operational stepped frequency microwave radiometer," *Monthly Weather Rev.*, vol. 135, no. 9, pp. 3070–3085, Sep. 2007.

[2] A. B. Tanner and C. T. Swift, "Calibration of a synthetic aperture radiometer," *IEEE Trans. Geosci. Remote Sens.*, vol. 31, no. 1, pp. 257–267, Jan. 1993.

[3] S. F. El-Nimri, W. L. Jones, E. Uhlhorn, C. Ruf, J. Johnson, and P. Black, "An improved C-band ocean surface emissivity model at hurricane-force wind speeds over a wide range of earth incidence angles," *IEEE Geosci. Remote Sens. Lett.*, vol. 7, no. 4, pp. 641–645, Oct. 2010.

[4] L. Hong, W. L. Jones, T. T. Wilheit, and T. Kasparis, "Two approaches for inter-satellite radiometer calibrations between TMI and WindSat," *J. Meteorol. Soc. Jpn.*, vol. 87A, pp. 223–235, 2009.

[5] D. P. Jorgensen and P. T. Willis, "A Z-R relationship for hurricanes," *J. Appl. Meteorol.*, vol. 21, pp. 356–366, 1982.

[6] R. L. Olsen, D. V. Rogers, and D. B. Hodge, "The aR^b relation in the calculation of rain attenuation," *IEEE Trans. Antennas Propag.*, vol. AP-26, no. 2, pp. 318–329, Mar. 1978.

[7] P. G. Black and C. T. Swift, "Airborne stepped frequency microwave radiometer measurements of rainfall rate and surface wind speed in hurricanes," in *Proc. 2nd Conf. Radar Meteorol.*, Zurich, Switzerland, 1984, pp. 433–438.

[8] S. S. Chen, J. F. Price, W. Zhao, M. A. Donelan, and E. J. Walsh, "The CBLAST-Hurricane program and the next-generation fully coupled atmosphere-wave-ocean models for hurricane research and prediction," *Bull. Amer. Meteor. Soc.*, vol. 88, no. 3, pp. 311–318, 2007.

[9] Private Communication With Eric Uhlhorn, NOAA/AOML/Hurricane Research Division, Miami, FL.

[10] [Online]. Available: ftp://ftp.nsstc.org/outgoing/lafonta/sst/grib2/conus/

[11] D. M. Le Vine, A. J. Griffis, C. T. Swift, and T. J. Jackson, "ESTAR: A synthetic aperture microwave radiometer for remote sensing applications," *Proc. IEEE*, vol. 82, no. 12, pp. 1787–1801, Dec. 1994.

[12] F. Ulaby, R. K. Moore, and A. K. Fung, *Microwave Remote Sensing, Active and Passive*, vol. 1. Norwood, MA: Artech House, 1981.

[13] R. A. Amarin, "Hurricane wind speed and rain rate measurements using the airborne hurricane imaging radiometer (HIRAD)," Ph.D. dissertation, Univ. Central Florida, Orlando, FL, 2010, EECS.

[14] E. W. Uhlhorn and P. G. Black, "Verification of remotely sensed sea surface winds in hurricanes," *J. Atmos. Oceanic Technol.*, vol. 20, no. 1, pp. 99–116, Jan. 2003.

Ruba A. Amarin (M'06) received the B.A. degree in electronic engineering from the Princess Sumaya University for Technology, Amman, Jordan, in 2004, M.S. degree in electrical engineering from the University of Central Florida, Orlando, in 2006, and the Ph.D. degree in electrical engineering from the University of Central Florida, Orlando, in 2010.

She is author or coauthor of approximately 30 publications.

W. Linwood Jones (SM'75–F'99–LF'09) received the B.S. degree in electrical engineering from the Virginia Polytechnic Institute, Blacksburg, in 1962, M.S. degree in electrical engineering from the University of Virginia, Charlottesville, in 1965, and the Ph.D. degree in electrical engineering from the Virginia Polytechnic Institute and State University in 1971.

He is currently a Professor with the Department of Electrical and Computer Engineering at the University of Central Florida in Orlando. At UCF, he teaches undergraduate and graduate courses in communications, satellite remote sensing and radar systems. Also, he is the Director of the Central Florida Remote Sensing Laboratory where he performs research in satellite microwave remote sensing technology development. Prior to becoming a College Professor in 1994, he had 27 years federal government employment with NASA at the Langley Research Center in Hampton, VA; at NASA Headquarters in Wash DC, and at the Kennedy Space Center, FL. Further, he spent eight years in the private aerospace industry with employment at General Electric's Space Division in King of Prussia, PA and Harris Corporation 's Government Aerospace Systems Division in Melbourne, FL.

Dr. Jones is a member of the American Geophysical Union and Commission F of the Union Radio Scientifique Internationale. For education, he received the IEEE Orlando Section: Outstanding Engineering Educator Award 2003, the College of Engineering: Excellence in Undergraduate Teaching Award 2004, the IEEE Florida Council: Outstanding Engineering Educator Award 2004, and the University of Central Florida: Outstanding Graduate Student Mentor Award 2011. For his research, he received four NASA Special Achievement Awards, seven NASA Group Achievement Awards, the CNES Space Medal, the Aviation Week and Space Technology Space Program Award-1993, and the Naval Research Lab 2004 Alan Berman Research Publications Award.

Salem Fawwaz El-Nimri (M'03) received the B.A. degree in electronic engineering from the Princess Sumaya University for Technology, Amman, Jordan, in 2004, M.S. degree in electrical engineering from the University of Central Florida, Orlando, in 2006, and the Ph.D. degree in electrical engineering from the University of Central Florida in 2010.

James W. Johnson (SM'80) received the B.S. and M.S. degrees in electrical engineering from Virginia Tech in Blacksburg, in 1966 and 1969, respectively. He began his career at the NASA, Langley Research Center in Hampton, VA, in 1966, initially conducting research in device technology at microwave and millimeter wave frequencies.

In the 1970s, he worked in the area of microwave remote sensing for earth sciences. He developed techniques for measuring ocean surface and polar ice characteristics using active and passive microwave systems. He served as the NASA project engineer for the development of the SeaSat Wind Field Scatterometer. During the 1980s, he led the Spacecraft Instrumentation Systems Section in the Flight Electronics Division at Langley. In the 1990s, he had responsibility for directing conceptual design studies in earth science applications for NASA's Mission to Planet earth. In recent years, he was Group Leader in the Electromagnetics and Sensors Branch responsible for developing advanced microwave radiometer technology, which included the Hurricane Imaging Radiometer for improving numerical modeling and forecasting of the intensity and track of hurricanes. He recently retired from NASA and is currently a Research Scientist with the Central Florida Remote Sensing Lab, University of Central Florida in Orlando.

Mr. Johnson is a member of the International Union of Radio Science. He is author or coauthor of approximately 50 publications. He has served on technical program committees for international conferences and as a reviewer for IEEE and American Geophysical Union publications.

Christopher S. Ruf (S'85–M'87–SM'92–F'01) received the B.A. degree in physics from Reed College, Portland, OR, and the Ph.D. degree in electrical and computer engineering from the University of Massachusetts, Amherst.

He is currently a Professor of atmospheric, oceanic, and space sciences; a Professor of electrical engineering and computer science; and Director of the Space Physics Research Laboratory at the University of Michigan, Ann Arbor. He has worked previously at Intel Corporation, Hughes Space and Communication, the NASA Jet Propulsion Laboratory, and Penn State University. In 2000, he was a Guest Professor with the Technical University of Denmark. He has published in the areas of microwave radiometer satellite calibration, sensor and technology development, and atmospheric, oceanic, land surface and cryosphere geophysical retrieval algorithms.

Dr. Ruf is a member of the American Geophysical Union (AGU), the American Meteorological Society (AMS), and Commission F of the Union Radio Scientifique Internationale. He has served on the editorial boards of the AGU *Radio Science*, the IEEE TRANSACTIONS ON GEOSCIENCE AND REMOTE SENSING (TGRS), and the AMS *Journal of Atmospheric and Oceanic Technology*. He is currently the Editor-in-Chief of TGRS. He has been the recipient of three NASA Certificates of Recognition and four NASA Group Achievement Awards, as well as the 1997 TGRS Prize Paper Award, the 1999 IEEE Resnik Technical Field Award, and the 2006 International Geoscience and Remote Sensing Symposium Prize Paper Award.

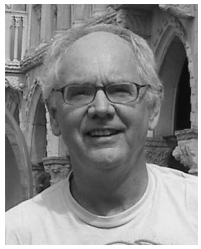

Timothy L. Miller received the A.B. degree in mathematics from Case Western Reserve University, Cleveland, Ohio, in 1972, M.S. degree in atmospheric science from the University of Arizona, Tucson, in 1979, and the Ph.D. degree in applied mathematics from the University of Arizona in 1982.

He is currently a Research Scientist for NASA at Marshall Space Flight Center, Huntsville, AL. At MSFC, he is Lead for the Research and Analysis Team in the Earth Science Office. His research areas are in weather systems and climate dynamics. Also, he is Principal Investigator for the Hurricane Imaging Radiometer (HIRAD), a passive microwave radiometer to make observations of wind speed and rain rate over the ocean surface. He was a member of the Laser Atmospheric Wind Sounder (LAWS) science team and was Mission Scientist for the NASA projects ATLAS 2 and 3 (Spacelab missions for atmospheric observations) and Project Scientist for the Space Readiness Coherent Lidar Experiment (SPARCLE).

Dr. Miller is a member of the American Meteorological Society (AMS) and the American Geophysical Union (AGU). He is a member of the AMS Committee on Satellite Meteorology. He has received several NASA awards, including the Medal for Exceptional Achievement and has published in several meteorological and fluid dynamics journals.

Eric Uhlhorn received the B.S. degree in meteorology from the Florida State University in 1993, the M.S. degree in physical oceanography from the Florida Institute of Technology in 1996, and the Ph.D. degree in meteorology and physical oceanography from the University of Miami, FL in 2008.

He is currently a Meteorologist at the Hurricane Research Division of the NOAA/Atlantic Oceanographic and Meteorological Laboratory in Miami.